Latin American Journal of Solids and Structures
www.lajss.org

Resistance and elastic stiffness of RHS "T" joints: part I - axial brace loading

Abstract

This paper presents a study on the behaviour of welded "T" joints between RHS sections under brace axial loading. A finite element model was developed to investigate the influence of some geometrical variables on the joint's response. The brace load (always in tension) was incremented up to joint failure, while the chord was kept unloaded. In the companion paper (part II) a complementary study including chord axial loading is presented. The force-displacement curves corresponding to the different geometries are analyzed and compared, focusing on the failure loads and elastic stiffness. Different failure criteria are discussed and applied to the present curves and a comparison of the numerical results with the Eurocode 3 provisions is presented and discussed.

Keywords

Finite element method; hollow section joints; deformation limit; plastic analysis; elastic stiffness.

R.M.M.P. de Matos[a]
L.F. Costa-Neves[b]
L.R.O. de Lima[c]
P.C.G.S. Vellasco[d]
J.G.S. da Silva[e]

[a]ISISE - Civil Engineering Department, University of Coimbra, Portugal
[b]INESCC, Civil Engineering Department, University of Coimbra, Portugal
[c,d,e]UERJ - State University of Rio de Janeiro, Brasil

Corresponding author:
[a]ruimatos@dec.uc.pt
[b]luis@dec.uc.pt
[c]luciano@eng.uerj.br
[d]vellasco@eng.uerj.br
[e]jgss@eng.uerj.br

http://dx.doi.org/10.1590/1679-78251790

Received 19.12.2014
Accepted 30.05.2015
Available online 07.07.2015

1 INTRODUCTION

The use of hollow sections is quite common in steel structures (Figure 1), partly due to their mechanical and aesthetical characteristics. The most common structural hollow sections are rectangular (RHS), square (SHS) or circular (CHS). The precision of design methods for these sections has a major importance considering the economical and safety points of view, and available analytical formulations to predict their behaviour have been included in modern design guides codes such as the EN 1993-1-8: Eurocode 3 (2005), hereafter referred as Eurocode 3 or EC3, the ISO 14346 (2013) that

is based on CIDECT design guide (Packer et al., 2009), and more recently the Brazilian ABNT NBR 16239 (2013) code.

Among the important issues to be dealt with in the analysis and design of hollow sections structures, is the characterization of the joints' behaviour. Recent studies of hollow sections structural joints point out for further research needs (Lima et al., 2008), especially when the chord failure mode changes from pure bending to bending and shear or to punching shear, where available analytical models for the prediction of the failure load may be unsafe or uneconomical.

The most common type of joint in hollow sections is the fully welded joint, as illustrated in Figure 1 and in Figure 2, that is quite simple and aesthetically appealing. One of the reasons for the popularity of this solution is the cumbersome access to the inside of the column, making bolted solutions more complex and costly. Alternative techniques that provide the connection from the outside only, such as the Flowdrill, Hollobolt and Hollofast, are available and were studied in the past, but do not cope, in general, with the desired resistance or stiffness - Costa-Neves (2004). These same limitations apply to simple endplate joints, and these facts justify the adoption of the fully welded solution in the current study.

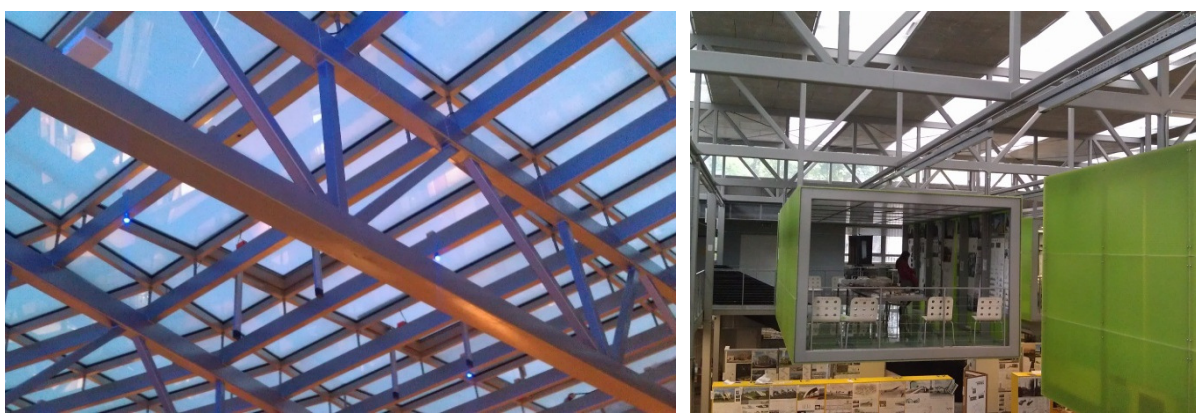

Figure 1: Examples of Hollow sections applications.

Figure 2 shows the geometry adopted in this study, known as "T- Joint", where the horizontal element is the chord, to which the vertical element, the brace, is fully welded. In this paper, the brace is submitted to axial tension loading, incremented up to joint failure.

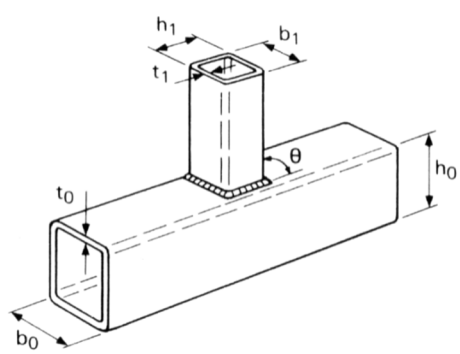

$$\beta = b_1/b_0$$
$$\mu_1 = b_1/t_1$$
$$\mu_0 = b_0/t_0$$
$$\gamma = b_0/(2t_0)$$

Figure 2: Welded T-joint.

It is known that the behaviour of this joint may be influenced by the stress state of the chord, and therefore the axial load in this element (most frequently present in current structures such as trusses) may be of some importance for a proper joint characterization. With this fact in mind, a companion paper, "Resistance and Elastic Stiffness of RHS "T" Joints: Part II - Combined Axial Brace and Chord Loading", deals with the interaction of these forces and its influence over the T-joint behaviour.

2 STUDIES ON THE BEHAVIOUR OF HOLLOW SECTIONS JOINTS

Three approaches have been adopted in the past to study joints between hollow section members: experimental, numerical, and analytical. Yu (1997) refers the study of Stewarts and Loyds in 1965 where some tests aiming at studying the resistance of such joints were carried out, and the first consistent study was performed by Jubb and Redwood (1966). However, the big boost in this field occurred only in the eighties of the 20th century, when a large number of studies were registered.

Korol and Mirza (1982) performed a numerical study with shell elements to evaluate the joints resistance; Yu (1997) studied the strength of multiple geometries of connections between rectangular hollow sections; Packer (1993); Packer and Henderson (2003) presented significant advances for predicting the plastic load of joints with the aid of yield lines mechanisms.

The geometrical parameters usually used to characterize the joint behaviour are illustrated in Figure 2, and dictate the response in terms of resistance and stiffness. Zhao and Hancock (1993); Zhao (2000) obtained the force-displacement or moment-rotation curves for a wide range of joints and have correlated the variation of those parameters with the joint's main features. They also proposed a deformation limit as a way to estimate the ultimate load of the joints, as discussed in section 5; Lu et al. (1993, 1994) carried out numerical and experimental studies on RHS joints with welded steel plates and concluded that the joint resistance increases as β increases and as μ or γ decrease. Similar conclusions were published by Cao et al. (1998a; 1998b); Kosteski and Packer (2000; 2001; 2003); Kosteski et al. (2003); Packer (1993); Packer and Henderson (2003); Wardenier et al. (2010) that deal with the manufacturing, design and assembly of tubular elements, joints and structures. Lie et al. (2006a; 2006b) performed experimental and numerical studies on this joint geometry with similar conclusions.

Costa-Neves (2004); Costa-Neves et al. (2004) studied experimentally the behaviour of joints between I-beams and RHS columns connected by endplates and welded bolts, and evaluated the accuracy of existing methods for predicting their resistance. They also proposed a model to evaluate the joints stiffness accounting for the column loaded face contribution.

In the T-joint geometry in Figure 2 the brace or beam transmits axial loading to the chord or column loaded face that is mobilized in bending and shear and is very frequently the critical component for the joint deformability and resistance, as accepted by most authors, e.g., Packer and Henderson (2003); Cao et al. (1998a); Kosteski et al. (2003); Costa-Neves (2004). This is also reflected in design codes/standards, e.g. EC3 (2005); ISO (2013), and justifies a special attention to this component.

The typical force-displacement curve (or moment-rotation curve) of the chord face is illustrated in Figure 3, as observed by many authors, namely Costa-Neves (2004); Lima et al. (2007; 2008); Matos (2008), and may be characterized by three different domains and by three major features: the

elastic domain characterized by the initial stiffness, $S_{j,ini}$; a second domain revealing a drop in stiffness as yielding begins and formation of a bending mechanism with a corresponding force F_{pl} when yielding is generalized; and the third domain reflecting the component behaviour after complete yielding and presenting a positive slope characterized by the membrane stiffness $S_{j,m}$. This membrane stiffness is revealed for slender RHS faces (i.e. for a large values of the μ_0 parameter – see Figure 2), as stated by Costa-Neves (2004).

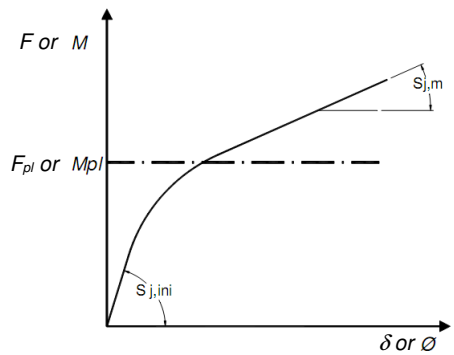

Figure 3: Typical force-displacement or moment-rotation curves for the RHS loaded face.

2.1 Resistance of the RHS loaded face

As a consequence of the behaviour shown in Figure 3, it may be quite hard to identify in a force-displacement curve or in a moment-rotation curve (obtained experimentally or numerically) the failure load F_{pl} or the failure moment M_{pl}. In fact, the membrane effect masks the onset of the yielding mechanism, except for thick faces where membrane action is negligible, as stated by Costa-Neves (2004). The awareness of this fact made some authors to develop alternative criteria to the plastic analysis or to the identification of a knee in a known force-resistance or moment-rotation curve.

A commonly used method to establish the resistance of the chord loaded face is the definition of a maximum allowable out-of-plane displacement for this component: Korol and Mirza (1982) proposed that the ultimate load or moment should correspond to rotations or displacements of 25 times their elastic limits, and since that generally corresponds to about 1.2 times the chord thickness ($1.2t_0$), the failure criterion proposed by these authors is $1.2t_0$; Kosteski et al. (2003) proposed a maximum displacement of 1% of the chord face, b_0 (see Figure 2); Lu et al. (1994); Zhao (2000) observed in some curves where the yield point could be more accurately identified that it was usually located between 2.5% and 4% of b_0 and proposed a maximum value for the displacement of 3% of the chord face. They also observed that when some curves corresponding to different tests are superposed, they intersect each other at a point of approximately 3% b_0. This last criterion is the most commonly used in the literature.

As an alternative to the maximum deformation method, Kosteski et al. (2003) defined the conventional yield point of the loaded face as the intersection of two lines adjusted to the elastic and to the membrane zones of the load-displacement curve, proposing a bilinear approach (Figure 4a) and the log approach (Figure 4b).

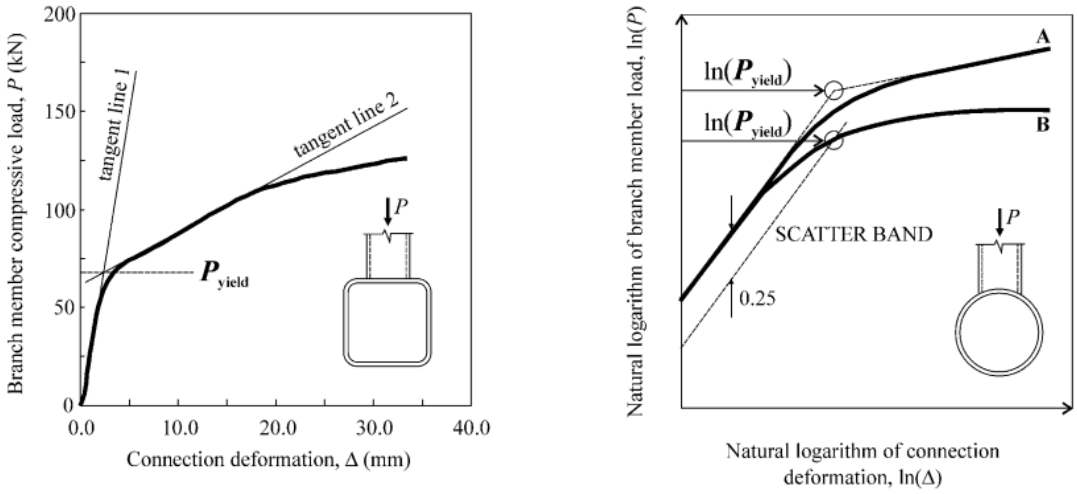

(a) Bilinear approach

(b) Logarithmic approach

Figure 4: Methodologies to derive the plastic load from force-displacement curves (Kosteski et al., 2003).

Plastic analysis remains an election method to derive the chord face resistance, assuming the formation of a yield line mechanism with corresponding plastic values F_{pl} or M_{pl} that are the failure chord face load or moment. This method naturally neglects any membrane action, and finding the most suitable mechanism is essential to derive the most accurate resistance prediction.

Many authors used this approach and proposed different shapes for the yield lines to obtain more accurate solutions for the plastic load in the context of RHS, I or H minor axis joints: Packer and Hendersen (2003); Packer et al. (2009); Zhao and Hancock (1993); Cao et al. (1998a; 1998b); Kosteski and Packer (2000; 2001; 2003); Kosteski et al. (2003); Wardenier et al. (2010) proposed mechanisms with straight lines or with 10 straight lines and circular sectors and also optimization strategies to define their position. Some of them accounted for shear and proposed pure punching shear mechanisms. Kosteski et al. (2003) concluded that for values of β greater than 0.7 punching shear influences the resistance and therefore proposed a punching shear line mechanism or combined mechanisms of bending and punching shear.

Gomes (1990) proposed an optimization for the yield lines composed by straight lines and log spiral segments, and the advantage of this new approach compared to straight lines mechanisms is highlighted in Figure 5. Also shown in this figure is the strong growth of the bending capacity as β increases, tending to infinity as β tends to 1. This naturally results in the failure by alternative failure modes, and if the chord face is involved, then failure is associated to shear and/or punching shear. The value of $\beta \leq 0.85$ is proposed in the Eurocode 3 (2005) as the limit for the predominance of chord face failure, and after which the formulas strictly based on bending mechanisms will give unsafe results.

2.2 Initial stiffness of the RHS loaded face

A quite limited number of authors studied in the past the initial or elastic stiffness ($S_{j,ini}$ shown in Figure 3) when the loaded face of a tubular section is involved. They have concluded that this feature strongly increases with the increase of the chord face thickness t_{wc}: Korol and Mirza (1982);

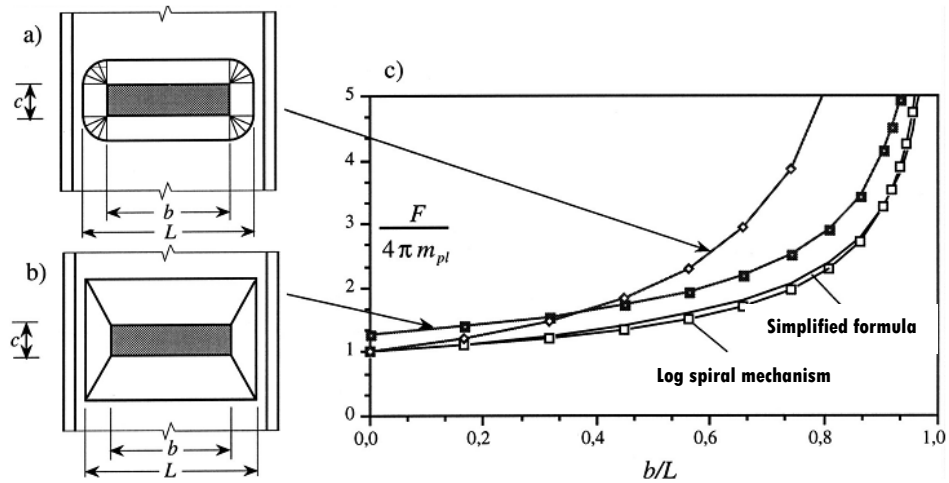

Figure 5: Comparison between log spirals and straight + circular lines mechanisms (Gomes, 1990).

Czechowski et al. (1987); Packer (1993); Costa-Neves (2004); Lima et al. (2007; 2008); Matos (2008). It increases also with the increase of the parameter β (related to the loaded area width) and more intensively for larger values of β, but decreasing with increasing bending flexibility at the borders of the plate: Czechowski et al. (1987); Costa-Neves (2004).

As far as the stiffness prediction is concerned, Packer (1993); Packer et al. (2009) state that this component's elastic stiffness should be evaluated experimentally or by finite element simulations.

Other authors established empirical equations to predict the initial stiffness of this component based on experimental or numerical results for specific cases: Korol and Mirza (1982) published abacuses to derive the initial stiffness of a particular RHS joint geometry based on the finite differences method; Szlendak (1996) proposed a similar expression for the initial stiffness of RHS faces with directly welded I-beams based on the results of 72 experimental tests; Fujita et al. (2001) proposed numerical expressions to derive non-linear moment-rotation curves including the initial and membrane stiffness as a combination of the joint geometrical parameters and Lima et al. (2007) proposed an expression to predict the initial stiffness of a particular minor axis joint (where the web behaviour is quite similar to the RHS loaded face) based on experimental tests and numerical simulations results.

A prediction of the initial stiffness as a function of the parameters showed in Figure 2 by more general analytical proposals based on physical models adjusted by numerical or experimental results were proposed by Czechowski et al. (1987); Costa-Neves (2004). Again, a common feature of all these observations and models is the fact that the elastic stiffness increases for larger values of β and for smaller values of μ and γ.

2.3 Membrane stiffness of the RHS loaded face

The third domain in Figure 3 reflects the component behaviour after the formation of a complete yielding mechanism and is characterized by the membrane stiffness $S_{j,m}$. This membrane stiffness leads to an over strength of the RHS face but may vanish in some circumstances, such as compression of the member containing the loaded face, or cyclic loading (Costa-Neves, 2004). This justifies the

fact that the membrane over strength should not be considered as a strength reserve but as a higher load level that may overstress other components of the joint such as bolts or welds, and should therefore be considered. This effect was observed experimentally and numerically by various authors, such as Gomes (1990); Lu et al. (1994); Kosteski and Packer (2001); Zhao (2000); Costa-Neves (2004); Costa-Neves et al. (2004); Lima et al. (2007; 2008); Matos (2008). The major conclusion from these studies is that membrane effect is more relevant for slender RHS faces (for large μ_0 parameter) - Costa-Neves (2004).

In the authors knowledge, the only existing analytical models to predict the membrane stiffness (and therefore the over strength of the component chord face) based on the joint geometry and the parameters in Figure 2 were proposed by Thornton (2002); Costa-Neves (2004).

3 EUROCODE 3 APPROACH

Eurocode 3 (2005) presents a design methodology for joints between hollow sections where only the resistance is accounted for, and that was more recently adopted by the Brazilian code ABNT NBR 16239 (2013). This methodology imposes the analysis of the relevant failure modes in Figure 6, and in Table 1 the relevant analytical equations to predict the resistance of the joint geometry in Figure 2 are indicated.

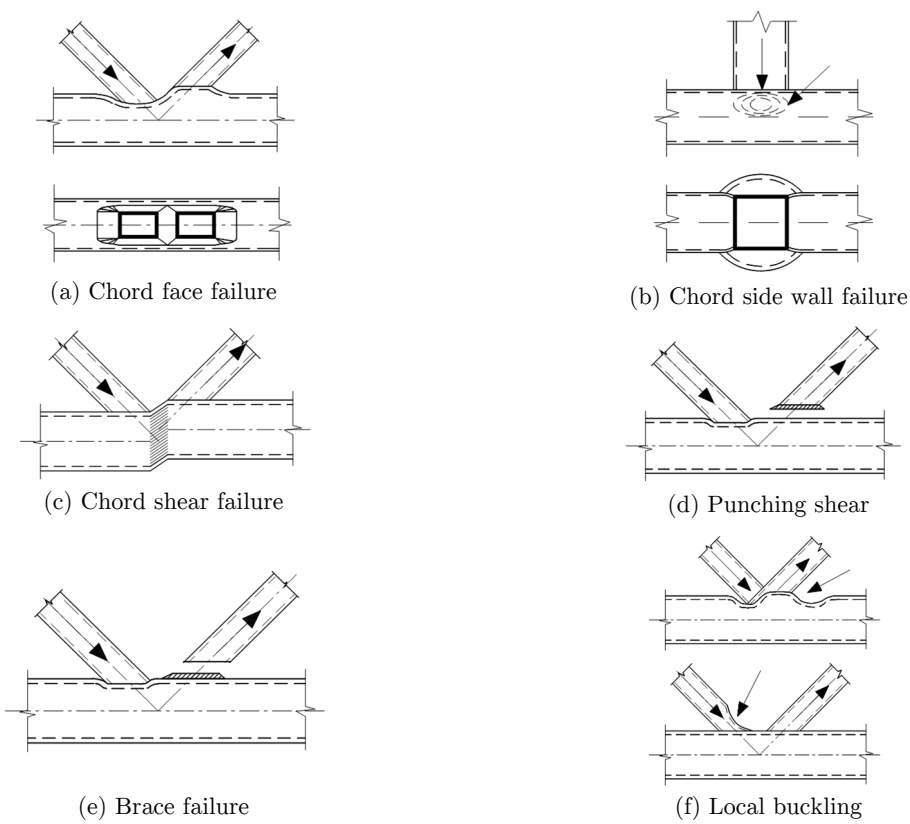

(a) Chord face failure

(b) Chord side wall failure

(c) Chord shear failure

(d) Punching shear

(e) Brace failure

(f) Local buckling

Figure 6: Failure modes - Eurocode 3 (2005).

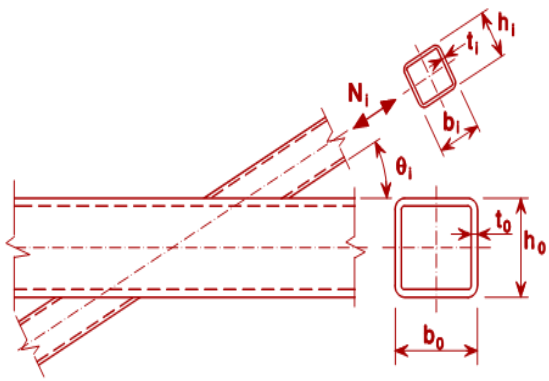

Design resistance $[i = 1]$

Chord face failure $\beta \leq 0.85$

$$N_{i,Rd} = \frac{k_n f_{y0} t_0^{\,2}}{(1-\beta)\sin\theta_i}\left(\frac{2\eta}{\sin\theta_i} + 4\sqrt{1-\beta}\right)\Big/\gamma_{M5}$$

Chord side wall buckling $\beta = 1$

$$N_{i,Rd} = \frac{f_b t_0}{\sin\theta_i}\left(\frac{2h_i}{\sin\theta_i} + 10t_0\right)\Big/\gamma_{M5}$$

Brace failure $\beta \geq 0.85$

$$N_{i,Rd} = f_{yi} t_i \left(2h_i - 4t_i + 2b_{eff}\right)\Big/\gamma_{M5}$$

Punching shear $0.85 \leq \beta \leq \left(1 - 1/\gamma\right)$

$$N_{i,Rd} = \frac{f_{y0} t_0}{\sqrt{3}\sin\theta_i}\left(\frac{2h_i}{\sin\theta_i} + 2b_{e.p}\right)\Big/\gamma_{M5}$$

For $0.85 \leq \beta \leq 1.0$ use linear interpolation between the value for chord face failure at $\beta = 0.85$ and the governing value for chord side wall failure at $\beta = 1.0$ (side wall buckling or chord shear).

For tension:

$$f_b = f_{y0}$$

For compression:

$$f_b = \chi f_{y0}$$

where χ is the reduction factor for flexural buckling obtained from EN 1993-1-1 using the relevant buckling curve and a normalized slenderness $\bar{\lambda}$ determined from:

$$\bar{\lambda} = 3.46\frac{\left(h_0/t_0 - 2\right)\sqrt{1/\sin\theta_i}}{\pi\sqrt{E/f_{y0}}}$$

$$b_{eff} = \frac{10}{b_0/t_0}\frac{f_{y0}t_0}{f_{yi}t_i}b_i \quad \text{but } b_{eff} \leq b_i$$

$$b_{e.p} = \frac{10}{b_0/t_0}b_i \quad \text{but } b_{e.p} \leq b_i$$

$n > 0$ (compression):

$$k_n = 1.3 - \frac{0.4n}{\beta} \quad \text{but } k_n \leq 1.0$$

$n < 0$ (tension):

$$k_n = 1.0$$

Table 1: EC3 (2005) methodology for the strength calculation of T joints between RHS.

The expressions presented by EC3 (2005) have a range of applicability requiring that the joints fulfil the following conditions: $\beta \geq 0.25$; $\mu_0 \leq 35$; $\mu_1 \leq 35$; and the chord is at least a class 2 section for pure bending.

4 NUMERICAL STUDY

4.1 Finite Element Model

Modelling by finite elements techniques require the development of a model that is at the same time accurate and simple enough not to consume to much computational resources in the context of parametrical studies, such as the case of the present study. A valid model is usually obtained if based in

the knowledge resulting from the previous experience as far as type of elements, analysis types and options, mesh densities, among others, are concerned. Additionally, the calibration of the model with experimental results is highly recommended.

In this study a numerical model accounting for material and geometrical nonlinearities using the ANSYS (2005) software was developed. Four nodes shell elements SHELL181 (Ansys, 2005) with six degrees of freedom per node were used, accounting for bending, shear and membrane deformations. The same major options were adopted by Korol and Mirza (1982); Lu et al. (1993; 1994); Lee (1999); Kosteski and Packer (2001); Fujita et al. (2001); Costa-Neves et al. (2004); Lima et al. (2007); Van der Vegte et al. (2010), among others, namely in what concerns the type of finite elements (shell instead of solid), model geometry (such as the section corners and welds modelling) or the analysis types and options described hereafter.

The mesh is depicted in Figure 7, being quite regular with well-proportioned elements to avoid numerical problems. At stress concentration areas and geometrical singularities a mesh refinement was implemented, as shown in the embedded details.

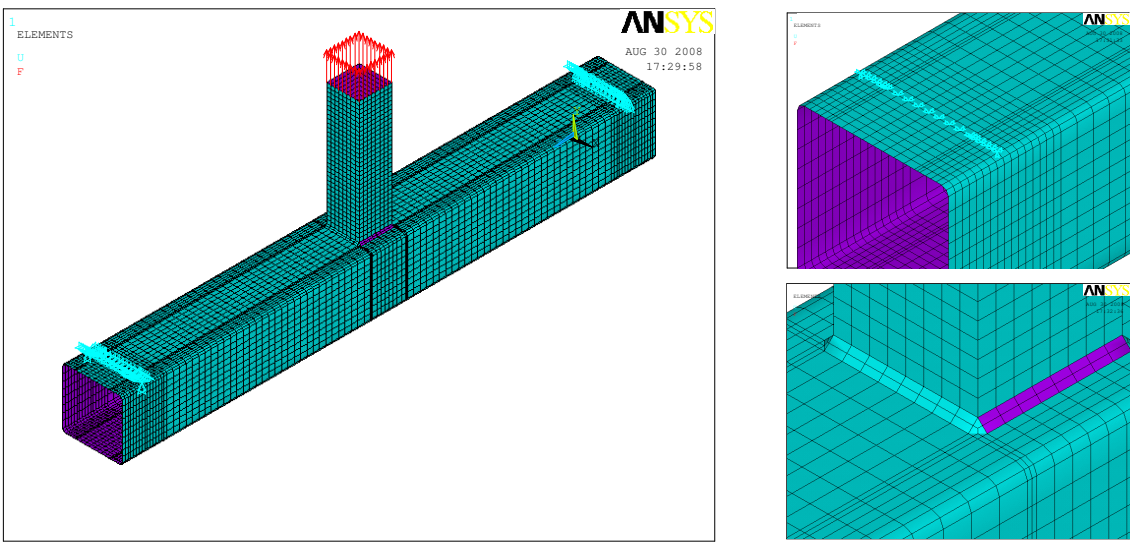

Figure 7: Overall view, root radius and weld of the numerical model for the analysis of the T joints.

The welds were modelled with shell elements as well (Figure 8), as proposed by Lee (1999), and later adopted by Lima et al. (2007; 2008), and where an adequate accuracy of results was obtained using this procedure. The inclined shell elements have the weld material properties while in their projection the connected members have unchanged properties.

This model (with few changes in the member cross section dimensions and material properties) was firstly adopted by the authors in Lima et al. (2007; 2008), where it was validated using the experimental results of Lie et al. (2006a). In the model validation all the details of the experimental test were simulated, including the geometrical and material properties of the elements (Table 2), and the experimental layout (span, supports, support stiffness). Figure 9 shows the comparison of the experimental (Lie et al., 2006a) and numerical curves. The dotted line in Figure 9 shows the predicted failure load obtained by the analytical method of EC3 (2005) (751 kN).

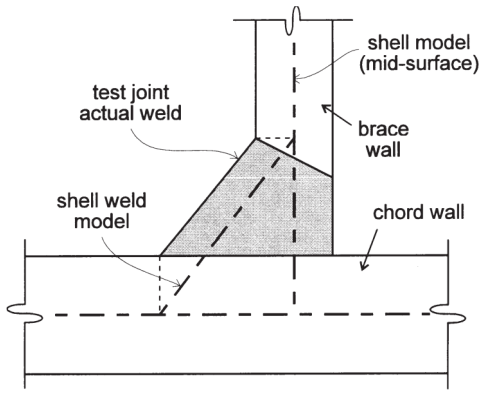

Figure 8: Weld modelling with shell elements (Lee, 1999).

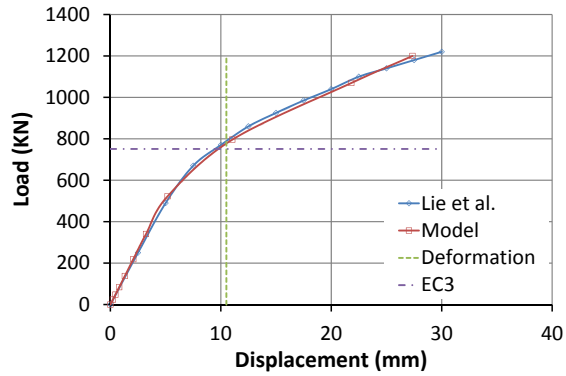

Figure 9: Numerical model validation.

b_0 (mm)	h_0 (mm)	t_0 (mm)	b_1 (mm)	h_1 (mm)	t_1 (mm)	t_w (mm)	f_y (MPa)	f_u (MPa)	f_w (MPa)
350	350	15	200	200	16	12	380.3	529.0	600.0

Table 2: Model geometrical and material properties.

4.2 Geometries

Having in mind that the parameters governing the behaviour of the joint in Figure 2 are related to the dimensions of the loaded area (the brace section dimensions) and to the dimensions of the loaded chord face (parameters β, μ and γ), a representative range of geometries was established - Table 3.

Chord (mm)	Brace (mm)	Brace loading
SHS 300x300xt t_w = 6, 8, 10, 12, 14, 16	SHS 100x100x12 SHS 150x150x12 SHS 180x180x12 SHS 220x220x12 SHS 250x250x12 SHS 260x260x12 SHS 285x285x12	Tension

Table 3: Description of the numerical simulations.

A cross section of 300x300 mm was adopted for the chord in this T geometry, and the parameter μ_0 was varied adopting different cross section thicknesses. Different brace sections were assumed to vary the parameter β. The brace was loaded in tension up to joint failure in all the 42 simulations (6x7x1) carried out, as indicated in Table 4, that also shows the variation in β (from 0.40 to 0.98) and in γ

(from 9.38 to 25). The designation E stands for the chord thickness, while M stands for the dimension of the brace cross section, with a constant thickness of 12 mm. As an example the designation E10 corresponds to a chord with a cross section thickness of 10 mm (300x300x10) while M180 corresponds to a brace with a cross section dimension of 180 mm (180x180x12). Consequently, the designation E10M180 stands for a joint of a 300x300x10 [mm] chord and a 180x180x12 [mm] brace.

	E6 ($\gamma=25$)		E8 ($\gamma=18.75$)		E10 ($\gamma=15$)		E12 ($\gamma=12.5$)		E14 ($\gamma=10.71$)		E16 ($\gamma=9.38$)	
	t_w	β	t_w	β	t_w	β	t_w	β	t_w	β	t_w	β
M100	12	0.40	12	0.40	12	0.40	12	0.40	12	0.40	12	0.40
M150	12	0.56	12	0.56	12	0.56	12	0.56	12	0.56	12	0.56
M180	12	0.66	12	0.66	12	0.66	12	0.66	12	0.66	12	0.66
M220	12	0.80	12	0.80	12	0.80	12	0.80	12	0.80	12	0.80
M250	12	0.90	12	0.90	12	0.90	12	0.90	12	0.90	12	0.90
M260	12	0.93	12	0.93	12	0.93	12	0.93	12	0.93	12	0.93
M285	10	1.00	8	0.99	6	0.98	6	0.98	5	0.98	4	0.97

Table 4: Geometrical parameters for each studied joint.

The parameter β is calculated according to Figure 2 but including the fillet weld influence., that has an effective width (considered as $0.8t_w$) added to the brace cross section width b_1; i.e. $\beta = \left(b_1 + 1.6t_w\right)/b_0$, according to Costa-Neves (2004).

This range of the geometrical parameters β, μ and γ was chosen to cover the most significant behaviour features identified in previous studies by Gomes (1990); Costa-Neves (2004). Specifically, small values of μ and γ lead to negligible membrane effect, and large values of β strongly increase the resistance obtained from pure bending mechanisms, and other phenomena need to be accounted for, as previously referred. Furthermore, for β values higher than 0.9, EC3 (2005) predictions are expected to be less accurate (Costa-Neves, 2004; Lima et al., 2008).

5 RESULTS

5.1 Finite element results

The numerical results for the resistance are shown in Table 5, resulting from the application of the 3% b_0 deformation criterion referred in section 2.1.2.

It is clear that the chord face resistance is strongly influenced by its thickness and strongly increases with the thickness increase (i.e. with the decrease of the parameter γ). The resistance is also strongly connected to the brace width, and increases with the increase of the parameter β, independently of the chord thickness.

Also indicated in Table 5 are the resistance values obtained from the EC3 (2005) based on plastic analysis, as well as the accompanying failures modes in Figure 6. Finally, the comparison between both methods is presented, expressed as the ratio of numerical and EC3 results, and the corresponding error as a percentage of the numerical value.

Geometry		β	γ	Num (kN)	EC3 (kN)	EC3 Failure mode	Num/EC3	Error (%)
	M100	0.40		71.89	82.70	(1)	0.87	-15.04
	M150	0.56		103.82	110.48	(1)	0.94	-6.42
	M180	0.66		135.14	138.70	(1)	0.97	-2.64
E6 (1*)	M220	0.80	25	209.60	214.11	(1)	0.98	-2.15
	M250	0.90		334.49	571.39	(2)	0.59	-70.83
	M260	0.93		364.63	767.37	(3)	0.48	-110.45
	M285	1.00		408.20	1341.90	(4)	0.30	-228.74
	M100	0.40		125.89	147.02	(1)	0.86	-16.78
	M150	0.56		177.21	196.41	(1)	0.90	-10.83
	M180	0.66		233.03	246.58	(1)	0.95	-5.82
E8 (1*)	M220	0.80	18.75	351.76	380.64	(1)	0.92	-8.21
	M250	0.90		475.26	866.44	(2)	0.55	-82.31
	M260	0.93		493.32	1080.00	(3)	0.46	-118.93
	M285	1.00		517.27	1781.92	(2)	0.29	-244.49
	M100	0.40		189.82	229.72	(1)	0.83	-21.02
	M150	0.56		270.83	306.90	(1)	0.88	-13.32
	M180	0.66		352.42	385.28	(1)	0.91	-9.32
E10	M220	0.80	15	508.92	594.75	(1)	0.86	-16.87
	M250	0.90		588.61	1213.79	(2)	0.48	-106.21
	M260	0.93		612.61	1421.05	(3)	0.43	-131.97
	M285	0.98		618.92	2192.85	(2)	0.28	-254.30
	M100	0.40		266.67	330.80	(1)	0.81	-23.78
	M150	0.56		372.55	441.93	(1)	0.84	-18.62
	M180	0.66		477.17	554.81	(1)	0.86	-16.27
E12	M220	0.80	12.5	626.80	856.45	(1)	0.73	-36.64
	M250	0.90		699.65	1613.43	(2)	0.43	-130.61
	M260	0.93		729.69	2003.44	(2)	0.36	-174.56
	M285	0.98		745.02	2730.35	(2)	0.27	-266.48
	M100	0.40		353.45	450.26	(1)	0.78	-27.39
	M150	0.56		492.37	601.52	(1)	0.82	-22.17
	M180	0.66		597.09	755.15	(1)	0.79	-26.47
E14	M220	0.80	10.71	734.39	1165.72	(1)	0.63	-58.73
	M250	0.90		823.46	2065.36	(2)	0.40	-150.81
	M260	0.93		833.92	2495.27	(2)	0.33	-199.22
	M285	0.98		840.26	3232.52	(2)	0.26	-284.70
	M100	0.40		449.01	588.10	(1)	0.76	-30.98
	M150	0.56		620.64	785.66	(1)	0.79	-26.59
	M180	0.66		743.23	986.32	(1)	0.75	-32.71
E16	M220	0.80	9.38	836.26	1522.57	(1)	0.55	-82.07
	M250	0.90		896.41	2569.59	(2)	0.35	-186.65
	M260	0.93		926.16	3032.21	(2)	0.31	-227.39
	M285	0.97		936.95	3758.29	(2)	0.25	-301.12

(1*) $\mu_0 > 35$ and section class > 2 for chord member

(1)-Chord face yielding; (2)-Interpolation; (3)-Chord punching shear; (4)-Chord side wall failure

Table 5: Numerical and analytical (EC3, 2005) results for each joint typology.

Table 6 shows the results obtained for the elastic stiffness in all tested geometries, highlighting that this feature increases in the same way as the resistance (with the thickness and with the brace width).

Geometry		Initial stiffness (kN/mm)	Geometry		Initial stiffness (kN/mm)
	M100	10.32		M100	43.22
	M150	18.38		M150	57.17
	M180	25.58		M180	65.25
E6	M220	36.16	E12	M220	74.05
	M250	41.93		M250	80.64
	M260	43.16		M260	84.14
	M285	46.01		M285	87.16
	M100	19.95		M100	55.18
	M150	31.37		M150	69.07
	M180	39.63		M180	76.72
E8	M220	49.77	E14	M220	84.85
	M250	54.96		M250	93.91
	M260	56.62		M260	98.95
	M285	59.86		M285	100.80
	M100	31.27		M100	66.82
	M150	44.54		M150	80.18
	M180	52.90		M180	87.32
E10	M220	62.36	E16	M220	94.87
	M250	67.17		M250	104.20
	M260	70.29		M260	105.40
	M285	74.40		M285	106.20

Table 6: Initial stiffness values for each joint typology.

More detailed information of the joints behaviour is depicted from the 42 force-displacement curves in Figure 10, highlighting the importance of the parameter β: for each of the six different chord thicknesses (where the parameters γ and μ are constant), the seven curves corresponding to the different brace dimensions (β values) are plotted. Also depicted in Figure 10 is the maximum displacement criterion of 3% b_0 referred in section 2.1.2 to establish the chord face ultimate limit state, represented by the continuous vertical lines and their corresponding intersection with the force-displacement curves.

The shape observed for all curves is the expected shape depicted in Figure 3, and it is possible to verify the above referred conclusions of the resistance and stiffness increase with the brace width increase. Also, smaller values of β allow larger membrane effect to arise, since shear and punching shear do not govern the behaviour. It is also possible to verify that for values of β larger than 0.8 this punching shear starts to govern, and no significant increase of resistance and even of stiffness may occur, except for small thicknesses (6 or 8 mm).

These trends for the stiffness and resistance as a function of β may as well be observed in Figure 11 and in Figure 12 where each curve represents respectively the stiffness and resistance variation with β for a constant thickness (constant parameter γ).

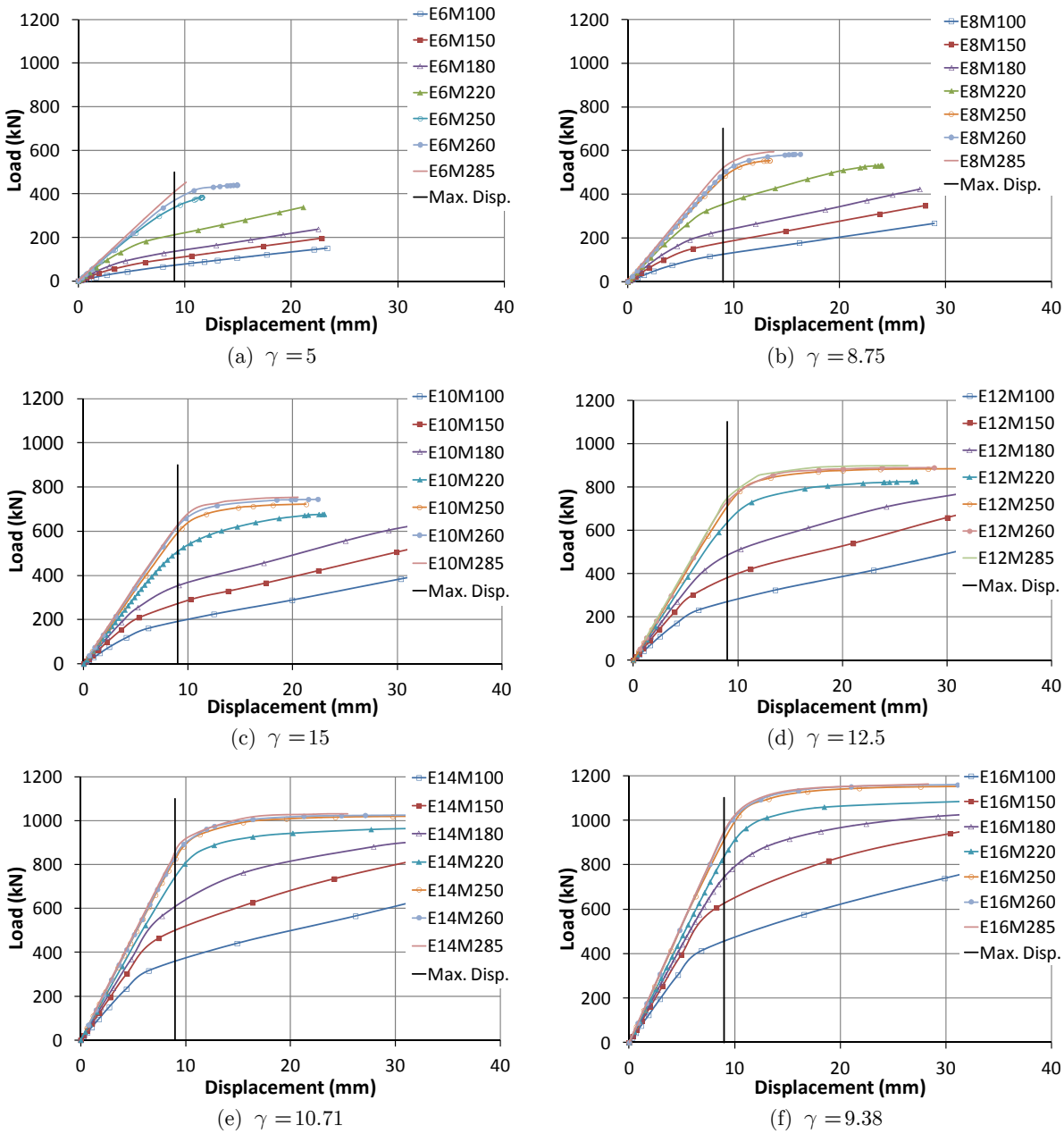

Figure 10: Force-displacement curves (β variation).

Figure 12 also shows the analytical results obtained from the application of the EC3 (2005) based on plastic analysis and their comparison to their numerical counterparts. It may be concluded that for values of $\beta \leq 0.66$ the results from both methodologies are quite close. However, when the value of β increases, EC3 starts to overestimate the resistance, being the values still similar if $\beta \leq 0.80$ but for a thickness up to 12 mm. For larger values of the chord thickness and for any thickness if $\beta > 0.80$, EC3 largely overestimates the joint strength if the above mentioned criterion of displacement limitation is used. Differences are up to four times comparing to the numerical resistance, but smaller differences would be obtained if other failure criteria were adopted.

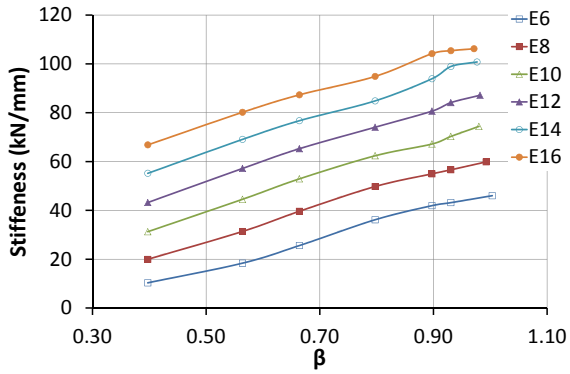

Figure 11: Initial stiffness (β variation).

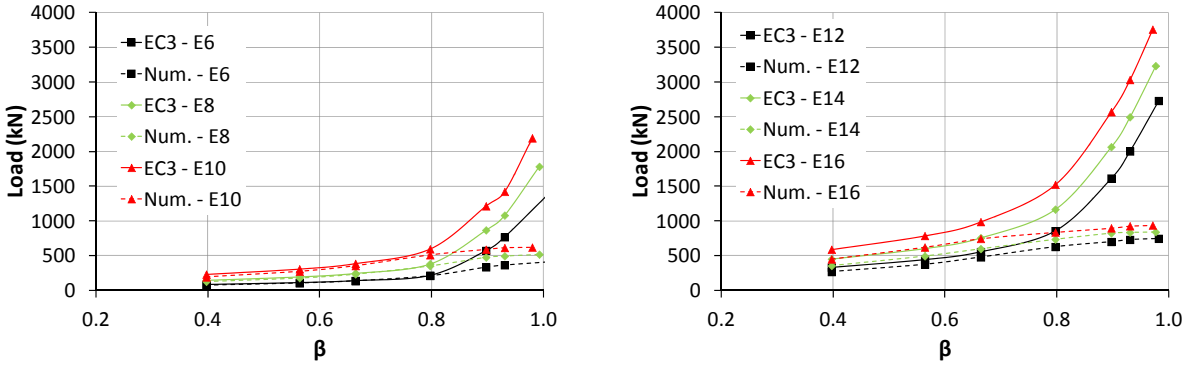

Figure 12: Comparison of numerical and EC3 (2005) resistances (β variation).

Highlighting the influence of the thickness over the joint behaviour may be expressed by the force-displacement curves in Figure 13, covering the different values of γ (different thicknesses) and where each group of curves relates to a constant chord width (constant value of β). As referred, the joint resistance and stiffness increase for increasing chord thicknesses (i.e. with the decrease of γ).

From Figure 13 it can also be concluded that when the thickness decreases the "knee" in the force-displacement curve starts to vanish, because membrane behaviour has a larger importance. Also, membrane effect is clearly of lesser significance for larger values of β (clearly larger than 0.8) and smaller values of γ (larger thicknesses), since it is linked to plate bending behaviour and for such values of β and γ punching shear or yielding of the chord lateral faces governs, instead of bending.

In a similar way as for β , these trends for the stiffness and resistance may now be plotted as a function of γ - Figure 14 and in Figure 15, where each curve shows the stiffness and resistance variation with γ for a constant brace-chord width ratio (constant β).

Again, a comparison of the analytical results from the EC3 (2005) to their numerical counterparts is plotted in Figure 15, but at this time highlighting the influence of the chord thickness: numerical resistance points are connected by a dotted line and EC3 resistance points are connected by a continuous line, for sake of clarity. Again, it is clear that for large values of β EC3 overestimates the strength, and this overestimation is much higher for small values of γ ($\gamma \leq 12.5$), i.e. for larger thicknesses, where shear is predominant.

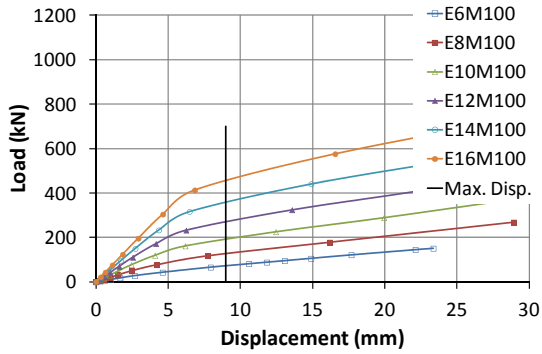

(a) $\beta = 0.40$

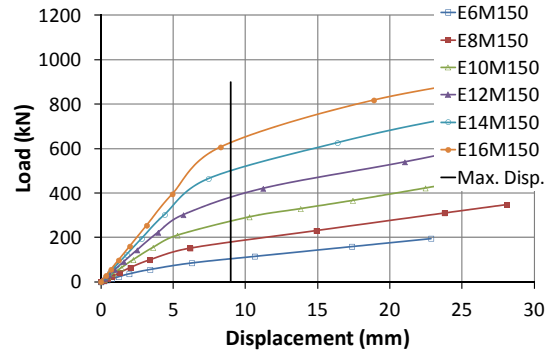

(b) $\beta = 0.56$

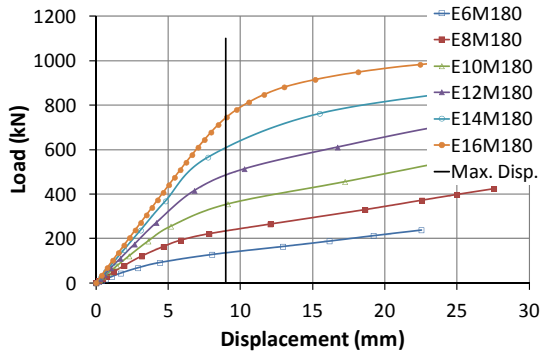

(c) $\beta = 0.66$

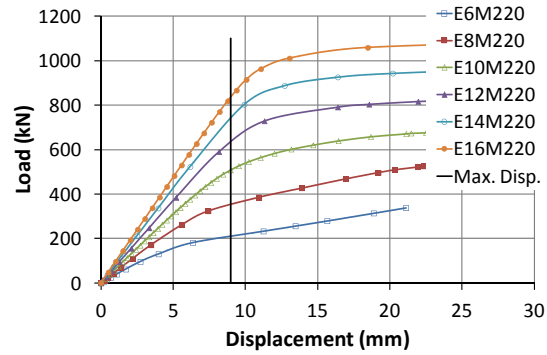

(d) $\beta = 0.80$

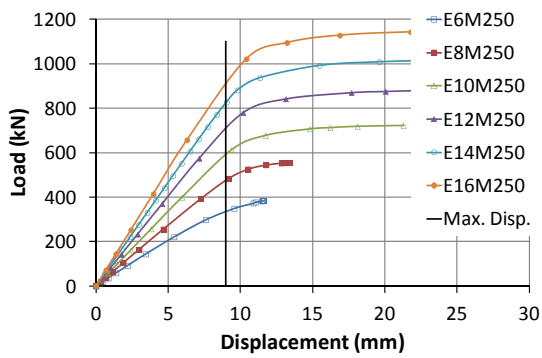

(e) $\beta = 0.90$

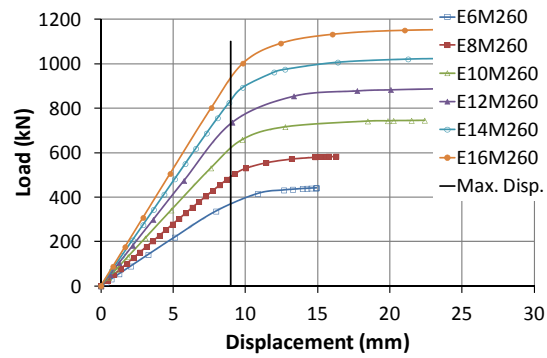

(f) $\beta = 0.93$

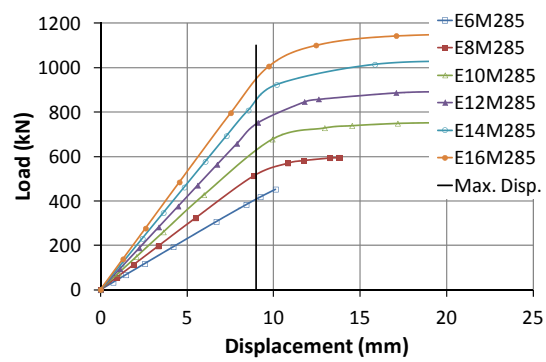

(g) $\beta = 0.97$ to 1.00

Figure 13: Force-displacement curves (γ variation).

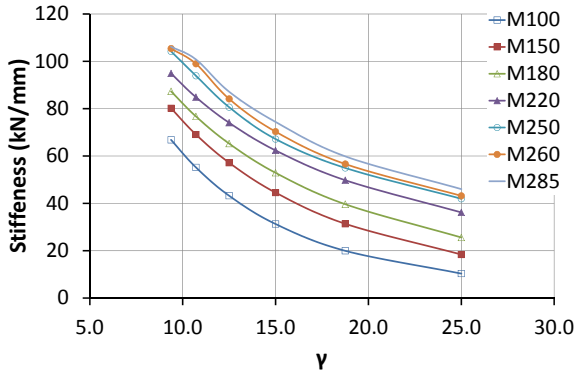

Figure 14: Initial stiffness (γ variation).

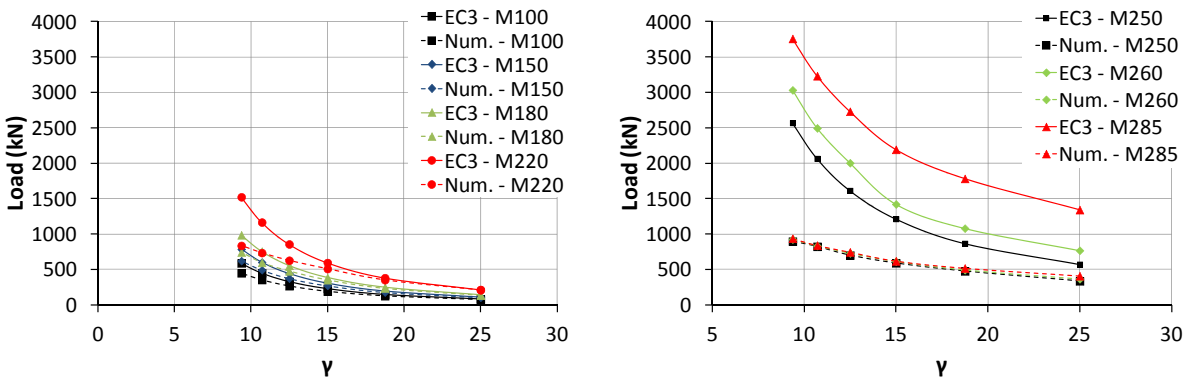

Figure 15: Comparison of numerical and EC3 (2005) resistances (γ variation).

Focusing on a particular joint stiffness, the joint of a 300x300x10 [mm] chord and a 180x180x12 [mm] brace (simulation E10M180), with parameters $\beta = 0.66$ (taking the weld contribution into account) and $\gamma = 15$, permits the illustration of the joint degradation up to failure, expressed not only by the load-deformation curves in Figures 10 and 13, but also by the yielding progress, in Figure 16, where the von Mises stresses are plotted for three different load levels: the first level (76.13 kN – Figure 16a) in the elastic range where the comparison stress is well below the yielding stress; the second level (at around 350 kN) corresponding to the point where Figure 10 and Figure 13 show a "knee" in the force-displacement curves - the numerical failure load from Table 5 is 352.42 kN), and where Figure 16b shows some yielding; and finally at a load level (662.4 kN) much higher than the plastic and failure load, but possible to attain due to membrane effects and to the spread of yielding to larger areas. As predicted by the Eurocode 3 (2005) the governing failure mode is, for this value of β , the chord face yielding that is also the first zone to suffer yielding, and the analytically predicted value of 385.3 kN (Table 5) is well in line with the numerical value of 352.42 kN

It may be concluded, in agreement with the conclusions of Packer and Cassidy (1995), that the weld does not present a uniform behaviour in the entire perimeter, having stress concentration at the corners.

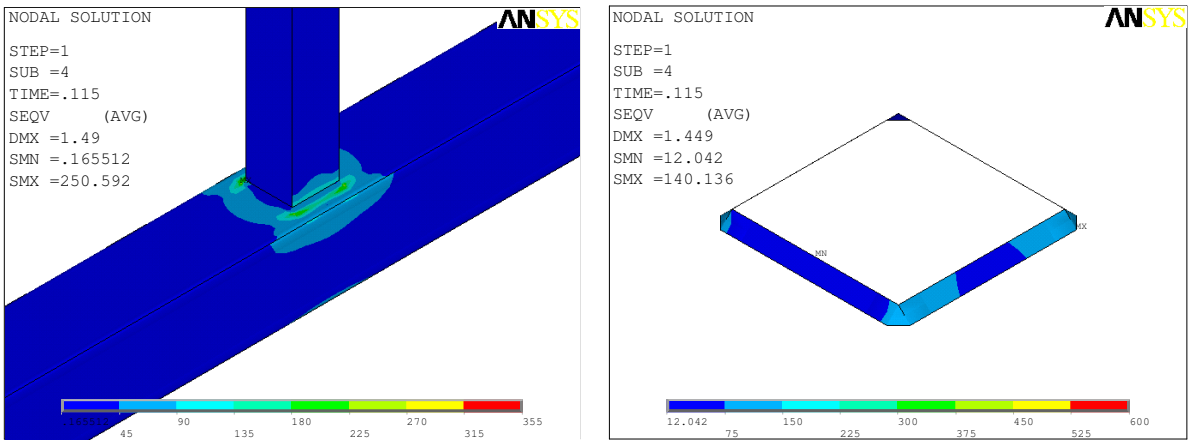

(a) Brace load 76.13 kN (tension)

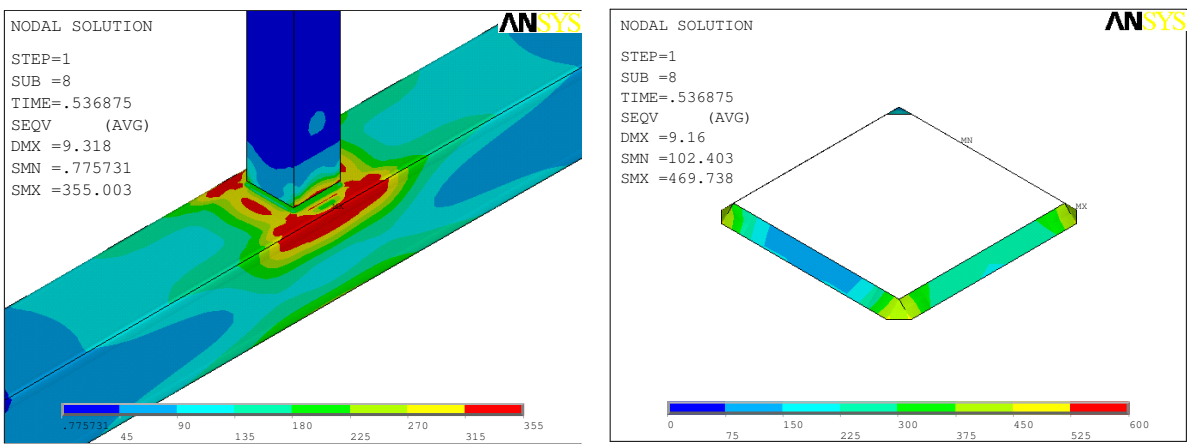

(b) Brace load 355.43 kN (tension)

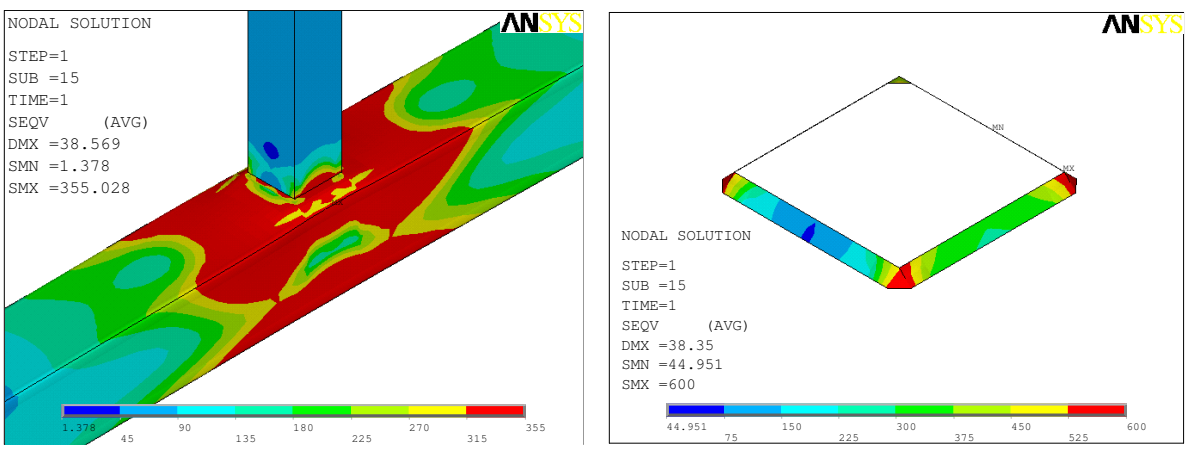

(c) Brace load 662.04 kN (tension)

Figure 16: Von Mises stress distribution at the joint and at fillet weld.

6 CONCLUSIONS

Recent studies questioning the applicability of the available analytical formulations based on yielding mechanisms to predict the behaviour of welded T-joints between RHS sections for some particular geometries justifies the need for further studies. This is the case for the formulation proposed in the Eurocode 3 (2005) for joints between hollow sections that account for several possible failure modes and is based on the plastic analysis for the chord face failure.

The need of alternative criteria to the plastic analysis or to the identification of a knee in a known force-displacement curve, made some authors (e.g. Lu et al., 1994; Zhao, 2000), to propose the chord face ultimate limit state as the force corresponding to a maximum displacement criterion of $3\%\ b_0$.

In this paper a finite element model using the ANSYS (2005) software was presented, and aims to study the behaviour of welded T- joints between RHS sections submitted to brace axial loading. In the companion paper (part II) a complementary study including chord axial loading and the interaction between both loadings is presented.

The numerical model was used to study the chord face behaviour when different dimensions of the loaded area and thickness of the loaded chord face are adopted, reflected in the variables β and γ. A total of 42 simulations were carried out with a variation in β from 0.40 to 0.98 and a variation in γ from 9.38 to 25.

The force-displacement curves for all the simulations were presented, highlighting the variation of the initial stiffness and the resistance with the relevant variables. The numerical results for the resistance derive from the application of the $3\%\ b_0$ deformation limit criterion and were compared to the EC3 (2005) results. For values of $\beta \leq 0.66$ both methodologies led to quite similar results, but when the value of β increased EC3 (2005) started to overestimate the resistance, being the values still similar if $\beta \leq 0.80$ but for a thickness not greater than 12 mm. For larger values of the chord thickness (for $\gamma \leq 12.5$) and for any thickness if $\beta > 0.80$, EC3 largely overestimated the numerical resistance. It should however be emphasized that the numerical values correspond to a limiting displacement criterion and not to a failure load involving an upper value in the force-displacement curve.

As a final note, it is remarked that the conclusions above expressed are in line with the numerical and experimental findings of several authors: Korol and Mirza (1982); Costa-Neves et al. (2004); Packer et al. (2009). On the other hand, the application of deformation criteria is applicable to the chord face and in strictness should be compared to the EC3 analytical results when chord face failure governs only. However, an attentive look at the force-displacement curves shows that, when this is not the case, the maximum numerical load is not much higher than the load resulting from that criterion, and therefore the conclusions would not be substantially different if another criterion to establish failure was used.

Acknowledgement

This work has been partially supported by the Portuguese Foundation for Science and Technology under project grant PEst-OE/ EEI/UI308/2014

References

ABNT NBR 16239, (2013). Design of steel and composite structures for buildings using hollow sections. Associação Brasileira de Normas Técnicas, São Paulo, Brazil (in portuguese).

Ansys 10.0 ®, (2005). ANSYS - Inc., Theory Reference.

Cao, J.J., Packer, J.A., Kosteski, N., (1998a). Design guidelines for longitudinal plate to HSS connections. Journal of Structural Engineering 1249(7): 784-791.

Cao, J.J., Packer, J.A., Young, G.J., (1998b). Yield line analysis of RHS connections with axial loads. Journal of Constructional Steel Research 48(1): 1-25.

Costa-Neves, L.F., (2004). Monotonic and cyclic behaviour of minor axis and tubular joints in steel and steel and concrete composite structures. PhD Thesis (in Portuguese), University of Coimbra, Portugal.

Costa-Neves, L.F., Silva, L.A.P.S., Vellasco, P.C.G., (2004). Experimental behaviour of end plate I-beam to concrete filled rectangular hollow section column joints. International Journal of Applied Mechanics and Engineering 9(1): 63-80.

Czechowski, A., Kordjak, J., Bródka, J., (1987). Flexibility formulae and modelling of joint behaviour in girders made of rectangular hollow sections. Proceedings of a state-of-the-art workshop on Connections and the Behaviour, Strength and Design of Steel Structures held at the ENS, Cachan, May, Elsevier Applied Science, London, pp. 175-182.

Eurocode 3, EN 1993-1-8: Eurocode 3 (2005). Design of steel structures Part 1.8: Design of joints. Brussels. CEN-European Committee for Standardization.

Fujita, K., Harada, Y., Morita, K., (2001). Evaluation of local rotational stiffness and strength of beam to column connection reinforced by increasing column thickness. Tubular Structures IX: Proc. of the Ninth International Conference on Tubular Structures, Dusseldorf, April, Ed. R. Puthli & S. Herion, Balkema, 483 - 492.

Gomes, F.C.T., (1990). Etat limite ultime de la résistance de l`âme d`une colonne dans un assemblage semi-rigide d`axe faible. Rapport Interne 203, MSM – Université de Liège.

International Organization for Standardization (ISO), (2013). Static Design Procedure for Welded Hollow-Section Joints - Recommendations, ISO 14346:2013(E), Geneva, Switzerland.

Jubb, J.E.M., Redwood, R.G., (1966). Design of joints to box sections. The Institution of Structural Engineers Conference on Industrialised Building and the Structural Engineer, UK.

Korol, R., Mirza, F., (1982). Finite element analysis of RHS T-joints. Journal of the Structural Division, ASCE 108(ST9): 2081-2098.

Kosteski, N., Packer, J.A., (2000). Bracing connections to rectangular HSS columns. Connections in Steel Structures IV – Behaviour Strength and Design, Proceedings Fourth International Workshop Oct 2000, Roanoke, Virginia, USA, AISC/ECCS, 2002, 788-797.

Kosteski, N., Packer, J.A., (2001). FEM evaluation of stiffened longitudinal branch plate-to-RHS member connection. Tubular Structures IX: Proc. of the Ninth International Conference on Tubular Structures, Dusseldorf, April, Ed. R. Puthli & S. Herion, Balkema, 145-154.

Kosteski, N., Packer, J.A., (2003). Welded Tee-to-HSS connections. Journal of Structural Engineering 129(2): 151-159.

Kosteski, N., Packer, J.A., Puthli, R.S., (2003). A finite element method based yield load determination procedure for hollow structural section connections. Journal of Constructional Steel Research 59: 453-471.

Lee, M.M.K., (1999). Strength, stress and fracture analyses of offshore tubular joints using finite elements. Journal of Constructional Steel Research 51: 265-286.

Lie, S., Chiew, S., Lee, C., Yang, Z., (2006a). Static strength of cracked square hollow section T joints under axial loads. I: Experimental, ASCE Journal of Structural Engineering 132(3): 368-377.

Lie, S., Chiew, S., Lee, C., Yang, Z., (2006b). Static strength of cracked square hollow section T joints under axial loads. II: Numerical, ASCE Journal of Structural Engineering 132(3): 378-386.

Lima, L.R.O., Neves, L.F.C., Silva, J.G.S., Vellasco, P.C.G.S., Andrade, S.A.L., (2007). Parametric analysis of RHS T joints under static loading. CC2007 - 11th International Conference on Civil, Structural and Environmental Engineering Computing, Saint Julians, Proceedings of the 9th International Conference on the Application of Artificial Intelligence to Civil, Structural and Environmental Engineering, Edinburgh, Civil Comp Press 1: 1-15.

Lima, L.R.O., Vellasco, P.C.G.S., Andrade, S.A.L., Silva, J.G.S., Neves, L.F.C., Bittencourt, M.C., (2008). Structural response of K and T tubular joints under static loading. International Workshop on Connections in Steel Structures, Chicago, Proceedings of the International Workshop on Connections in Steel Structures, AISC - American Institute of Steel Construction 1: 1-10.

Lu, L.H., Puthli, R.S., Wardenier, J., (1993). Semi-rigid connections between plates and rectangular hollow section column. Proceedings of the Fifth International Symposium on Tubular Connections held at Nottingham, UK, August, E & FN Spon, London, 723-731.

Lu, L.H., de Winkel, G.D., Yu, Y., Wardenier, J., (1994). Deformation limit for the ultimate strength of hollow section joints. 6th International Symposium on Tubular Structures, Melbourne, 341-347.

Matos, R., (2008). Avaliação Paramétrica de Nós de Geometria "T" de Perfis Tubulares. MsC Thesis (in Portuguese), University of Coimbra, Portugal.

Packer, J.A., (1993). Moment connections between rectangular hollow sections. Journal of Constructional Steel Research 25: 63-81.

Packer, J.A., Cassidy, C., (1995). Effective weld length for HSS T, Y, and X connections. Journal of Structural Engineering 121(10): 1402-1408.

Packer, J.A., Henderson, J.E., (2003). Hollow structural section, connections and trusses. Canadian Institute of Steel Construction, Ontario, Canada. ISBN 0-88811-086-3.

Packer, J.A., Wardenier, J., Zhao, X.-L., van der Vegte, G.J., Kurobane, Y., (2009). Design guide for rectangular hollow section (RHS) joints under predominantly static loading 3(2), CIDECT.

Szlendak, J., (1996). Classification system for I-beam to RHS column connections. Tubular Structures VII: Proceedings of the Seventh International Symposium, Farkas, J. et al ed., Rotterdam, Balkema, Miskolc, Hungary, 245-252.

Thornton, W., (2002). A membrane method for transversely loaded column webs. Connections in Steel Structures IV – Behaviour Strength and Design, Proceedings 4th International Workshop Oct 2000, Roanoke, Virg, USA, AISC/ECCS.

Van der Vegte, G.J., Wardenier, J., Puthli, R.S., (2010). FE analysis for welded hollow section joints and bolted joints. Proceedings of the Institution of Civil Engineers, Structures and Buildings 163(6): 427-437.

Wardenier, J., Packer, J.A., Zhao, X-L., van der Vegte, G.J, (2010). Hollow sections in structural applications. 2nd Edition, CIDECT.

Yu, Y., (1997). The static strength of uniplanar and multiplanar connections in rectangular hollow sections. PhD Thesis, Delft University, Netherlands.

Zhao, X., Hancock, G., (1993). Plastic Mechanism analysis of T-joints in RHS subject to combined bending and concentrated force. Proceedings of the Fifth International Symposium on Tubular Connections held at Nottingham, UK, August, E & FN Spon, London, 345-352.

Zhao, X., (2000). Deformation limit and ultimate strength of welded T-joints in cold-formed RHS sections. Journal of Constructional Steel Research 53: 149-165.